NeuroImage 109 (2015) 368–377

Contents lists available at ScienceDirect

NeuroImage

journal homepage: www.elsevier.com/locate/ynimg

# Rhythmic 3–4 Hz discharge is insufficient to produce cortical BOLD fMRI decreases in generalized seizures

Mark W. Youngblood [a], William C. Chen [a], Asht M. Mishra [a,b], Sheila Enamandram [a], Basavaraju G. Sanganahalli [b,c], Joshua E. Motelow [a], Harrison X. Bai [a], Flavio Frohlich [e], Alexandra Gribizis [a], Alexis Lighten [a], Fahmeed Hyder [b,c,d], Hal Blumenfeld [a,b,e,f,*]

[a] Department of Neurology, Yale University School of Medicine, 333 Cedar Street, New Haven, CT 06520, USA
[b] Core Center for Quantitative Neuroscience with Magnetic Resonance (QNMR), New Haven, CT 06520, USA
[c] Department of Diagnostic Radiology, Yale University School of Medicine, 333 Cedar Street, New Haven, CT 06520, USA
[d] Department of Biomedical Engineering, Yale University School of Medicine, 333 Cedar Street, New Haven, CT 06520, USA
[e] Department of Neurobiology, Yale University School of Medicine, 333 Cedar Street, New Haven, CT 06520, USA
[f] Department of Neurosurgery, Yale University School of Medicine, 333 Cedar Street, New Haven, CT 06520, USA

ARTICLE INFO

*Article history:*
Accepted 25 December 2014
Available online 3 January 2015

*Keywords:*
Absence seizures
Consciousness
Epilepsy
Default mode network
Petit mal
EEG–fMRI
Negative BOLD

ABSTRACT

Absence seizures are transient episodes of impaired consciousness accompanied by 3–4 Hz spike–wave discharge on electroencephalography (EEG). Human functional magnetic resonance imaging (fMRI) studies have demonstrated widespread cortical decreases in the blood oxygen-level dependent (BOLD) signal that may play an important role in the pathophysiology of these seizures. Animal models could provide an opportunity to investigate the fundamental mechanisms of these changes, however they have so far failed to consistently replicate the cortical fMRI decreases observed in human patients. This may be due to important differences between human seizures and animal models, including a lack of cortical development in rodents or differences in the frequencies of rodent (7–8 Hz) and human (3–4 Hz) spike–wave discharges. To examine the possible contributions of these differences, we developed a ferret model that exhibits 3–4 Hz spike–wave seizures in the presence of a sulcated cortex. Measurements of BOLD fMRI and simultaneous EEG demonstrated cortical fMRI increases during and following spike–wave seizures in ferrets. However unlike human patients, significant fMRI decreases were not observed. The lack of fMRI decreases was consistent across seizures of different durations, discharge frequencies, and anesthetic regimes, and using fMRI analysis models similar to human patients. In contrast, generalized tonic–clonic seizures under the same conditions elicited sustained postictal fMRI decreases, verifying that the lack of fMRI decreases with spike–wave was not due to technical factors. These findings demonstrate that 3–4 Hz spike–wave discharge in a sulcated animal model does not necessarily produce fMRI decreases, leaving the mechanism for this phenomenon open for further investigation.


## Introduction

Absence seizures are a form of generalized epilepsy that present as brief staring spells marked by an abrupt 3–4 Hz spike-and-wave discharge on electroencephalography (EEG). These events can occur up to hundreds of times per day and may disrupt normal cognitive and psychosocial development in children (Camfield and Camfield, 2002; Crunelli and Leresche, 2002; Wirrell et al., 1996, 1997). Although effective medical treatments are available, this is not a benign condition because a substantial proportion of patients have persistent deficits in attention even when seizures are not occurring, and about 30% will not outgrow their seizures (Camfield and Camfield, 2002; Wirrell et al., 1997). To improve treatment of absence seizures, it is necessary to understand the fundamental pathophysiology of associated changes in brain networks. This effort has been greatly advanced in recent years by simultaneous EEG–functional magnetic imaging (fMRI), which has provided maps of brain activity changes associated with absence seizures. Interestingly, the most consistent cortical change observed in these studies has been blood oxygenation level-dependent (BOLD) fMRI decreases in widespread regions, including the default mode network (Aghakhani et al., 2004; Archer et al., 2003; Salek-Haddadi et al., 2003). The fMRI decreases persist for over 20 s after seizures end and do not fit the expected hemodynamic response function for the brief EEG discharges (Bai et al., 2010; Carney et al., 2010). Thus, although fMRI maps of brain activity in human absence seizures are available, the most prominent and consistent cortical changes remain unexplained.

* Corresponding author at: Yale Depts. of Neurology, Neurobiology, and Neurosurgery, 333 Cedar Street, New Haven, CT 06520-8018. Tel.: +1 203 785 3865; fax: +1 203 737 2538.
*E-mail address:* hal.blumenfeld@yale.edu (H. Blumenfeld).

http://dx.doi.org/10.1016/j.neuroimage.2014.12.066
1053-8119/

Because fMRI signals are only indirectly related to neuronal activity and in some cases can be misleading (Mishra et al., 2011; Schridde et al., 2008), it is crucial to investigate the relationship between fMRI changes in absence seizures and underlying neurophysiology to correctly interpret BOLD fMRI mapping. Animal models have provided some insights into these relationships. For example, direct multi-unit and local field potential recordings in rodent models have shown that cortical and thalamic fMRI increases are associated with transient increases in neuronal action potential firing and synaptic activity during spike–wave seizures, as expected (Mishra et al., 2011; Nersesyan et al., 2004a, 2004b). However, animal models have yet to shed light on the mechanism of cortical fMRI decreases that predominate in human studies. This may be because previous rodent and non-human primate models have only inconsistently shown cortical fMRI decreases, and they are typically minor compared to the widespread decreases observed in humans (Brevard et al., 2006; David et al., 2008; Mishra et al., 2013, 2011; Nersesyan et al., 2004a, 2004b; Tenney et al., 2003; Tenney et al., 2004a, 2004b).

There are a number of possible explanations for why animal models have so far failed to replicate the widespread cortical fMRI decreases seen in human studies. One important factor that could influence neuronal activity and cortical fMRI signals is that the spike–wave discharge frequency in human absence seizures is typically 3–4 Hz, whereas it is 7–8 Hz in most rodent models (Depaulis and van Luijtelaar, 2005; Motelow and Blumenfeld, 2009; Sitnikova and van Luijtelaar, 2007). Other interspecies differences from humans such as the lack of sulci and gyri in rodents and marmosets, and the lack of intrinsic inhibitory neurons in the ventroposterior thalamic nuclei of rats (Barbaresi et al., 1986) may also play a role.

To address the potential contributions of these factors to the lack of fMRI decreases we sought to develop a new animal model with 3–4 Hz spike–wave seizures more closely resembling human patients. Studies in non-lisencephalic animals such as felines (Prince and Farrell, 1969) have been more successful in replicating the 3–4 Hz electrographic activity observed in humans. Ferret thalamic slices have also been shown to spontaneously generate 3–4 Hz spike-and-wave discharges when exposed to gamma-aminobutyric acid A ($GABA_A$) antagonists *in vitro* (Blumenfeld and McCormick, 2000; Lee et al., 2005; von Krosigk et al., 1993). We therefore decided to administer a $GABA_A$ antagonist to ferrets *in vivo* to develop a new model of spike–wave seizures that more closely resembles human patients. This approach enabled us to investigate a number of possible contributing factors to fMRI decreases, including typical 3–4 Hz discharges, presence of cortical sulci and gyri, various anesthetic regimens, duration and amplitude of seizures, comparison to larger tonic–clonic seizures, and use of model-based and timecourse analysis methods similar to human studies.

## Methods

All experimental procedures were approved by the Yale University Institutional Animal Care and Use Committee and are in agreement with the National Institutes of Health Guide for the Care and Use of Laboratory Animals. Neuroimaging experiments were performed on adult female ferrets (*Mustela putorius furo*) obtained from Marshall BioResources and housed for a minimum of 3 days prior to use. EEG–fMRI data were obtained during seizures from 17 animals, and data were selected for analysis from 13 animals (425 g ± 70) based on appropriate blood gas and systemic parameters in the physiological range as described previously (Englot et al., 2008; Schridde et al., 2008) .

### *Animal preparation and surgery*

All animals underwent initial sedation in an induction chamber ventilated with 3–4% isoflurane. Following tracheostomy and initiation of artificial ventilation (70% $N_2O$, 30% $O_2$), anesthesia was continued with either 0.5–3.0% isoflurane or intramuscular injections of ketamine/xylazine (30/1 mg/kg). In one experiment, isoflurane was supplemented with intravenous injections of 2% α-chloralose solution. Depth of anesthesia was monitored using heart rate, blood pressure, and scalp electroencephalogram (EEG). To reduce movement artifact during neuroimaging experiments, paralysis was induced using intravenous injections of D-tubocurarine chloride (0.5 mg/kg).

An intravenous femoral line was installed for anesthetic and experimental injections. Continuous monitoring of arterial blood pressure and heart rate was facilitated through cannulation of a femoral artery. This line was also used to collect blood samples for periodic evaluation with an ABL 5 blood gas analyzer (Radiometer Analytical, Lyon, France). Physiological values ($pO_2$, $pCO_2$, and pH) were maintained as in prior studies (Mishra et al., 2011; Schridde et al., 2008) through adjustment of respiration rate and intravenous injections of sodium bicarbonate solution. Body temperature was recorded with a digital rectal probe and maintained at 37 °C using a warm-water heating pad.

### *Experimental procedures*

Bench electrophysiology experiments were performed to develop spike–wave and tonic–clonic seizure models using ferrets. These methods were replicated during subsequent neuroimaging experiments. Carbon-filament electrodes (1 mm) were installed subcutaneously for the measurement of scalp EEG as described previously (Mishra et al., 2011). The electrodes were oriented in the coronal plane over frontal and occipital regions. Electrographic signals were acquired in differential mode, amplified (×100) and filtered (1–30 Hz) using a Model 79D Data Recording System (Grass Instruments Co., Quincy, MA). A CED Micro 1401 with Spike 2 software (Cambridge Electronic Design, Cambridge, UK) was used to digitize EEG data at a 1000 Hz sampling rate for later analysis.

A custom-designed plastic holder was used for head fixation at the center of the surface coil during fMRI recordings. Each experimental session included multiple seizure episodes. Seizures were induced by intravenous injection of the $GABA_A$ antagonist bicuculline (0.12 mg/kg ± 0.01 for spike–wave seizures or 0.27 mg/kg ± 0.05 for tonic–clonic seizures). All MR data were obtained on a modified 9.4 T system with a Varian (Agilent Technologies, Santa Clara, CA) spectrometer using a custom-built $^1H$ radiofrequency surface coil (5 by 3 cm coil diameter). During fMRI recordings, the ferret was positioned prone in a specially designed plastic holder in such a manner that the modified surface coil would be at the top of the ferret's head. The magnetic field homogeneity was optimized by localized shimming to yield a typical water spectrum line-width of less than 20 Hz across the slices. High resolution anatomical scans were acquired using fast spin-echo contrast multi-slice sequences (FSEMS). For each animal 10, 15, or 20 slices were captured in the coronal plane with the following parameters: repetition time (TR) = 4 s, echo time (TE) = 20 ms, field of view (FOV) = 32 × 32 mm, matrix size = 128 × 128, for an in-plane resolution of 500 × 500 μm and slice thickness = 1000 or 2000 μm (no gap).

The custom surface head coil used for these experiments allowed excellent signal/noise ratio fMRI data acquisition for the cortex (SNR > 30) but not of deeper subcortical structures. BOLD signal was acquired using either spin-echo echo-planar imaging (8 animals) or gradient-echo echo-planar imaging (4 animals). Functional MRI measurements were performed with 10, 15 or 20 coronal slices in the same plane as anatomical images, using the following parameters: TR = 2000 ms, TE = 34 ms, FOV = 32 × 32 mm, 64 × 64 matrix size resulting in an in-plane resolution of 500 × 500 μm and slice thickness = 1000 or 2000 μm (no gap). The slices were acquired over 2000 ms, followed by a 1 or 2 s pause before the next image onset so that EEG could readily be interpreted during data acquisition as described previously (Mishra et al., 2011; Nersesyan et al., 2004a, 2004b); time between onset of consecutive image acquisitions was therefore 3 or 4 s. Between 300 and 900 images were acquired per

run, resulting in an imaging time per run that ranged from 20 to 60 min. The average number of seizures for each run was 2.26 seizures ± 0.30 (SEM). Images from the first 60 s of each run were discarded from analysis. In sessions with multiple seizures per run, the average inter-ictal time was 247.03 ± 53.9 (SEM) seconds.

*EEG data analysis*

In order to reduce artifacts during MRI pulse sequences, all EEG data were processed with a low-pass filter as described previously (Englot et al., 2008; Nersesyan et al., 2004a, 2004b). The processed EEG traces were used to determine onset and offset times of each seizure period. Seizures were first classified according to morphology, with spike–wave seizures being defined by regular spike-and-wave complexes and tonic–clonic seizures by tonic polyspike discharges and rhythmic polyspike and wave followed by postictal attenuation. Spike–wave seizures were further classified by duration, with seizures lasting ≤30 s classified as "short spike–wave", and seizures >30 s classified as "long spike–wave". This threshold was chosen to include all events with a duration similar to clinical absence seizures (typically 4 to 20 s long; Crunelli and Leresche, 2002; Ebersole et al., 2014) in a single group. A total of 18 short spike–wave, 17 long spike–wave and 35 tonic–clonic seizures were analyzed. Seizures of indeterminate or mixed morphology were excluded.

To investigate the periodicity of seizure activity, the sample autocorrelation function was calculated using data sampled from the first 20 s of each seizure (or less if the seizure duration was ≤20 s) by applying the "autocorr" function in MATLAB 8.1 (The MathWorks, Inc., Natick, MA). Lags of 0 to 500 ms, incrementing by 1 ms, were used. To avoid contamination of the autocorrelation function by MRI artifact, EEGs were first segmented into 2 s artifact-contaminated and 2 s artifact-free windows, and the first 1 s of each artifact-free window was used to calculate the autocorrelation function. Thus all quantitative EEG analyses were performed using data from the artifact-free segments. The autocorrelation of these artifact-free seizure windows was averaged to yield a within-seizure autocorrelation function. Finally, within-seizure autocorrelation functions were averaged across seizures to yield the within-animal autocorrelation function. As a criterion for periodicity we next calculated the sum of the square autocorrelation values from 100 ms to 500 ms lag for each animal; larger values for this criterion indicate more highly periodic signals and zero represents a completely aperiodic signal. A criterion value of 5 cleanly separated the EEGs into spike–wave and tonic–clonic seizure groups, and the fundamental oscillation frequency was only obtained for the more periodic spike–wave seizure group. Fundamental oscillation frequency was determined for each animal by using the time of the peak autocorrelation function at lag ≥ 100 ms and taking the reciprocal.

*Functional MRI data analysis*

fMRI data were processed using SPM 8 (Statistical Parametric Mapping, Wellcome Department of Imaging Neuroscience, Functional Imaging Laboratory, London, UK), as well as in-house software written in MATLAB by the authors (J.E.M, W.C.C., M.W.Y). Co-registration of images was performed across high-resolution anatomical images and the same transformations were then applied to the corresponding functional images. Slices along the anterior–posterior axis of each animal were manually chosen to match a set of 10 coronal template anatomical slices from an animal selected with high SNR. Of these 10 slices 7 were common to all data sets and were used in the final analysis. Registration between each slice and the corresponding template slice was then performed with a script in MATLAB using the two-dimensional "imregister2" function, with options set to use gradient descent optimization for a linear, intensity-based affine co-registration.

Each registration was visually verified by overlaying the registered and template images. In four animals, field inhomogeneity artifacts and low SNR caused anatomical images to be poorly registered by the automated process. In these cases, images were co-registered using a custom MATLAB script for manual linear scaling, rotation and translation of an overlaid image. After co-registration, fMRI images were spatially smoothed in SPM8 using a Gaussian kernel with a full width at half maximum of 0.25 mm. All analysis performed in SPM8 used co-registered, smoothed images.

In order to apply the same methods employed in analysis of human fMRI, data were analyzed using the standard general linear model (GLM) approach in SPM8, as well as using ROI-based timecourse analyses. The time series of each voxel was high-pass filtered (cutoff = 1/128 Hz). BOLD responses were related to seizures by regression with an ideal response, which was obtained by convolving the canonical hemodynamic response function (HRF) with a boxcar function equal to the seizure duration. Because the HRF of ferrets has not been studied extensively, we chose to use the standard canonical HRF provided by SPM8, which has been previously used in rodents (David et al., 2008). We considered several other variables that could potentially affect the results but did not include them as regressors in the analysis. For example, because center-of-mass analysis of the images did not reveal appreciable movement in the paralyzed animals we did not include motion-related regressors. Similarly heart rate, respiration and global BOLD signal did not systematically vary over the time scales in which the transient seizure events occurred, so these variables were also not included in the regression.

A standard first level, fixed-effects model was used to generate both single-animal and group level activation maps. All t-maps were corrected for false discovery rate (FDR) to the $p < 0.05$ level. Extent threshold k was 0 voxels. The sizes of significant clusters were reported by SPM in units of voxels k (voxel dimensions 0.5 × 0.5 × 1.0 mm). The total number of significant voxels was calculated by summing the sizes of all significant clusters. The percentage of significant voxels showing decreases was calculated within animal and for the grouped fixed-effect analyses. Due to the small sample size in the three groups ($n = 4, 6, 7$ animals for short spike–wave, long spike–wave, and tonic–clonic seizures, respectively), a more stringent random effects analysis revealed no statistically significant BOLD responses after FDR correction.

In order to more thoroughly investigate discharge-related fMRI increases or decreases, we repeated the analysis by replacing the canonical HRF with a gamma function that peaked at 3, 5, 7, or 9 s after seizure onset. This approach ensured that changes in BOLD signal that were time-locked to EEG activity would be investigated across a range of hemodynamic delays (Aghakhani et al., 2004; Bagshaw et al., 2004). Gamma probability-distribution-functions were generated in SPM8 with the same FWHM as the positive portion of the canonical HRF. The time-to-peak was varied for each curve as described above. All data were re-analyzed using the same methods as before, but now utilizing gamma functions with varied offsets. We then selected the gamma function with the maximum percentage of voxels showing cortical decreases, similar to prior uses of this approach for identifying maximal changes in human spike–wave seizures (Aghakhani et al., 2004).

Finally, to directly investigate the temporal evolution of fMRI changes in each seizure classification without assumptions of any model, BOLD response timecourses were generated for several cortical regions-of-interest (ROIs) using in-house MATLAB scripts. Polygon masks were drawn on the template brain for each of four ROIs (frontal cortex, cingulate cortex, lateral cortex, and medial posterior cortex; see Fig. 5A). BOLD timecourses were then calculated using the coregistered data within each ROI. Percent BOLD change was calculated for each seizure as 100 × (signal − baseline) / baseline where the signal was the average ROI BOLD value at each time point and baseline was the average across a 20 s preictal baseline period. BOLD timecourses for each ROI were then averaged across seizures between −100 s to +400 s around ictal onset. Most seizures had several minutes between them. For seizures

that were more closely spaced, time points from the postictal periods that overlapped the start of the next seizure were discarded. In addition, any pre-ictal time points (−100 s to 0 s) that occurred within 20 s of a preceding seizure end were discarded.

Average peak BOLD % change was calculated for each seizure type based on a 20 s time period that corresponded to the maximum response during the ictal window. The 20 s interval used for each seizure type was determined based on the peak response of the averaged timecourse data. For short spike–wave seizures, 10–30 s after ictal onset was found to have the maximum response when all seizures were averaged together, so that time period was used to calculate peak response for each individual seizure. For long spike–wave 40–60 s after onset was used, and 20–40 s after onset was used for TC seizures. Unless otherwise noted, all results are reported as mean ± SEM, and a significance threshold of $p < 0.05$ is used. Statistical tests are two-tailed unless otherwise noted. Corrections for multiple comparisons are described when applicable.

## Results

### *Ferret spike–wave seizure model*

Building upon earlier work demonstrating 3–4 Hz spike–wave activity in ferret thalamic slices (Blumenfeld and McCormick, 2000; Kim et al., 1997; von Krosigk et al., 1993), we began by attempting to recapitulate this activity in an *in vivo* model. Small intravenous injections of bicuculline (0.12 mg/kg ± 0.01) during initial electrophysiology experiments outside the MRI scanner were found to reliably produce rhythmic spike–wave firing in the cortex. These seizure events included slow waves punctuated by spike cortical discharges at approximately 3–4 Hz (Fig. 1A, and inset). Some seizures were also observed at 5–8 Hz (Fig. 2). Ictal onset and offset were marked by an abrupt change in EEG amplitude and frequency, with an electrographic morphology that resembled the spike–wave discharges seen in human childhood absence epilepsy (Ebersole and Pedley, 2003).

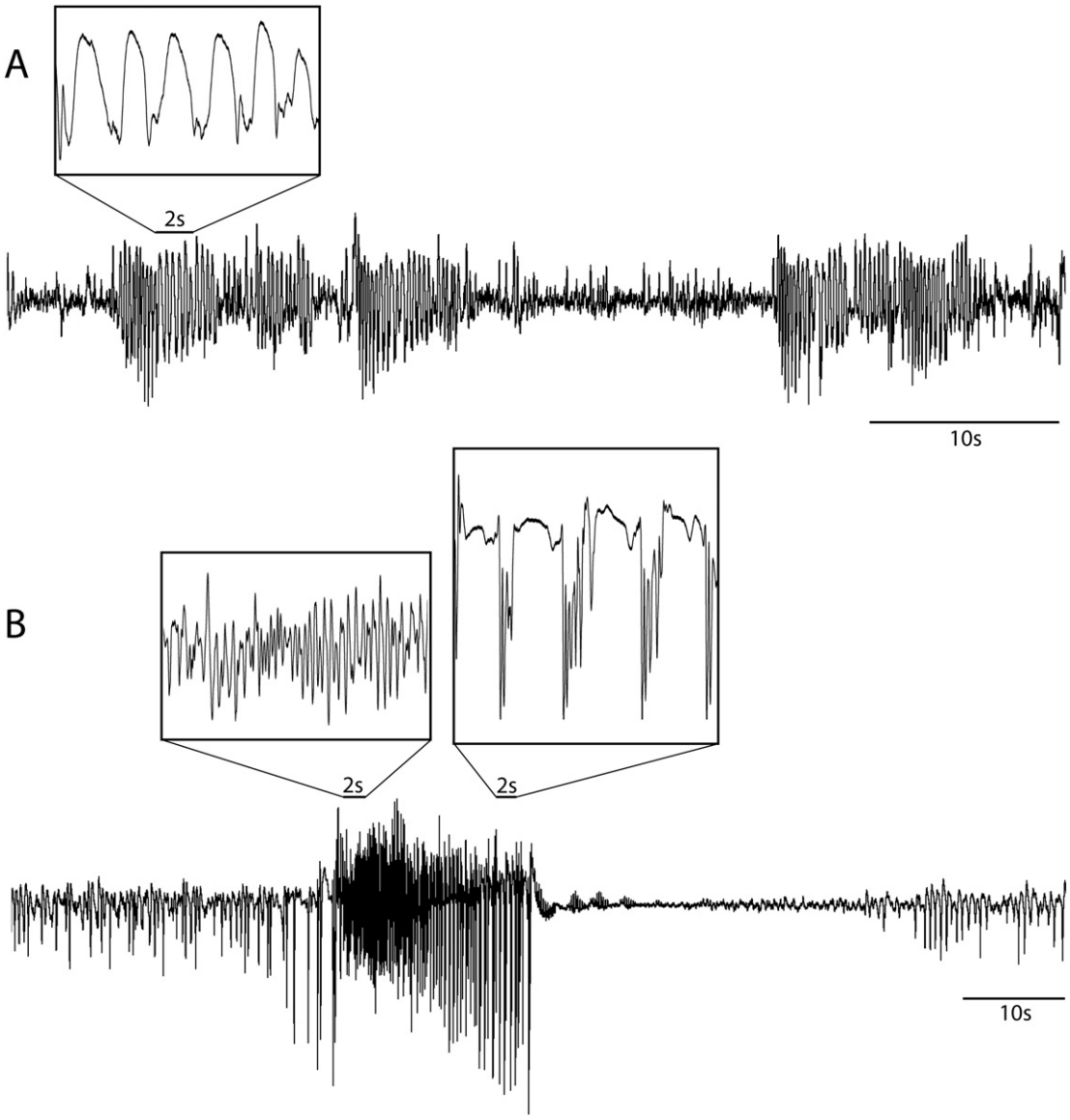


**Fig. 1.** Generalized seizures induced by intravenous injections of the $GABA_A$ antagonist bicuculline. Examples are shown from bench electrophysiology experiments. The dosage of bicuculline determined the type of seizure induced. (A) Smaller bicuculline injections generated 3–4 Hz spike–wave discharge. (B) Larger injections produced tonic–clonic episodes. Insets at higher time resolution show typical 3–4 Hz spike–wave morphology (A), or polyspike evolving into polyspike and wave in tonic–clonic seizures (B).

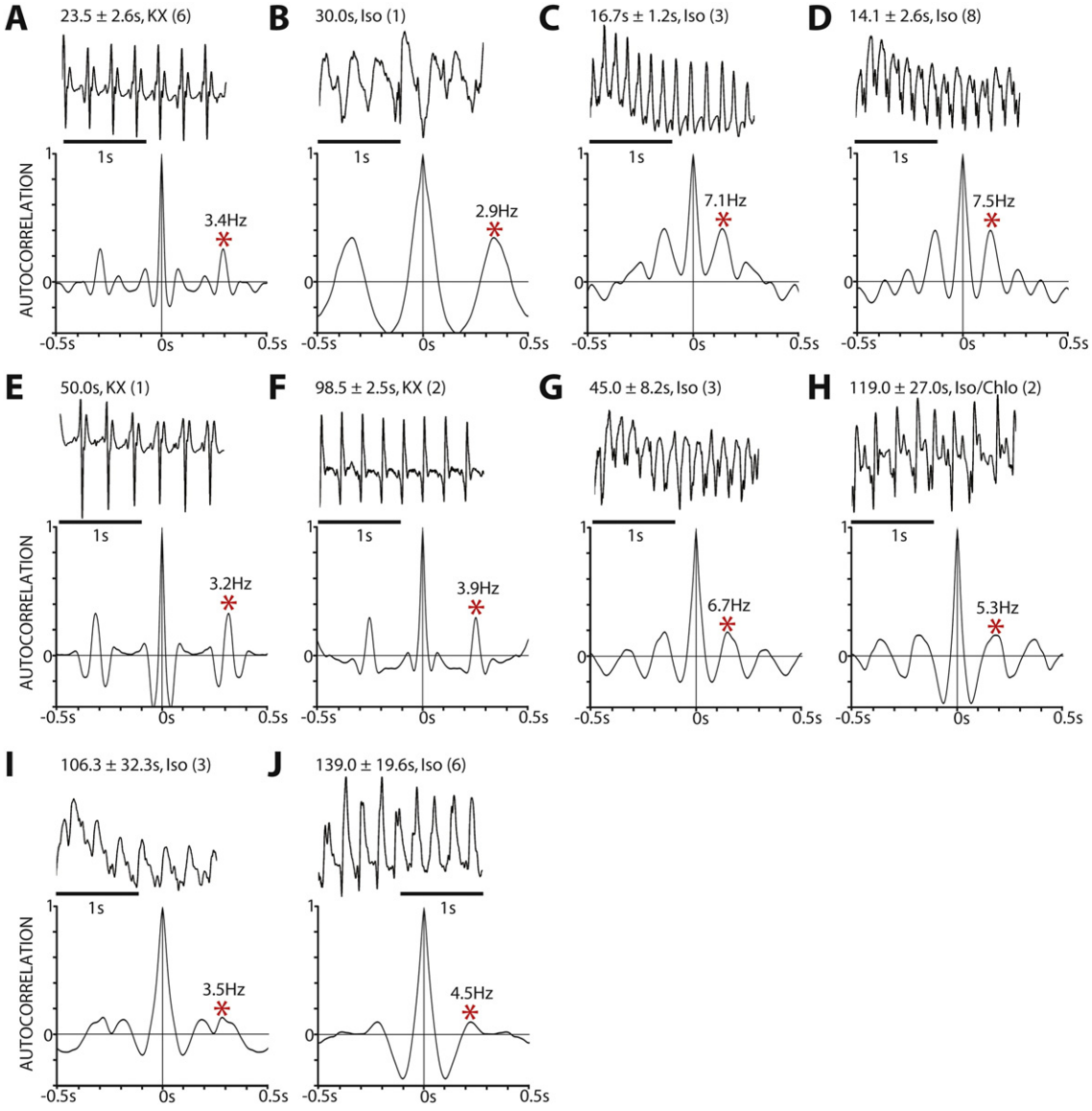


**Fig. 2.** Spike–wave seizures during EEG–fMRI experiments. (A–D) Short spike–wave seizures (duration ≤ 30 s) were observed in 4 animals, with mean duration of 18.6 s ± 1.8. (E–J) Long spike–wave seizures (duration > 30 s) were seen in 6 animals, with mean duration of 104.3 s ± 12.3. Each panel represents data from one animal, indicating mean seizure duration ± SEM for that animal, anesthetic used (Iso, isoflurane; KX, ketamine/xylazine, Iso/Chlo, isoflurane-alpha-chloralose), and number of seizures (in parentheses). EEG traces show 2 s of representative spike–wave discharges from each animal. Lower traces show mean autocorrelation during all spike–wave seizures within each animal with a lag of 0 to 500 ms (see Methods for details). Red asterisk * denote the peak autocorrelation point with lag ≥ 100 ms, and the corresponding peak frequency is displayed. Animals A, B, E, F, I, J had lower frequency, 2.9–4.5 Hz discharges, while animals C, D, G, H had higher frequency, 5–8 Hz discharges.

In contrast, higher doses of bicuculline (0.27 mg/kg ± 0.05) induced EEG activity that resembled human tonic–clonic seizures (Fig. 1B). These episodes began with a rapid onset of high-frequency tonic polyspike discharges followed by a transition to lower-frequency, polyspike and wave activity (Fig. 1B, insets). Post-ictal periods following tonic–clonic seizures were marked by attenuation in signal on EEG that often lasted several minutes.

Subsequent experiments were performed with simultaneous recordings of EEG and fMRI (Fig. 2). The EEG morphology showed some variation across animals, as is seen also in human patients (Seneviratne et al., 2012), but the predominant pattern for the lower doses of bicuculline was of generalized 3–4 Hz spike–wave (Fig. 2). Spike–wave seizures were found to be bimodally distributed with respect to duration. Consequently we divided our data into two groups for further analysis. A total of 18 "short" spike–wave seizures occurred across 4 animals, with an average seizure duration of 18.6 s ± 1.8 (mean ± SEM; range 6 to 30 s). Representative EEGs of seizures from this group are shown in Figs. 2A–D with corresponding autocorrelograms. A second group of "long" spike–wave seizures included 17 episodes across 6 animals (Figs. 2E–J). These events had an average seizure duration of 104.3 s ± 12.3 (mean ± SEM; range 34 to 195 s). In most cases seizures were induced using bicuculline in the presence of the anesthetic isoflurane, however similar seizures were also seen in three animals where the anesthetic ketamine/xylazine was used (Figs. 2A, E, F) and in one animal where a combination of isoflurane and α-chloralose was used instead (Fig. 2H).

Periodicity was evaluated by autocorrelograms (see Methods) revealing that spike–wave seizures in most animals had a fundamental frequency of 2.9 to 4.5 Hz (Figs. 2 A, B, E, F, I, J), whereas four animals had seizures of slightly higher frequency (Figs. 2C,D, G, H). Fundamental frequency was not significantly different in the short spike–wave and long spike–wave groups.

With higher doses of bicuculline, we obtained 35 tonic–clonic seizures in 7 ferrets (Fig. 3). Compared to spike–wave episodes, tonic–clonic seizures tended to exhibit power spectrum increases over a broader range of frequencies (data not shown) and were less periodic.

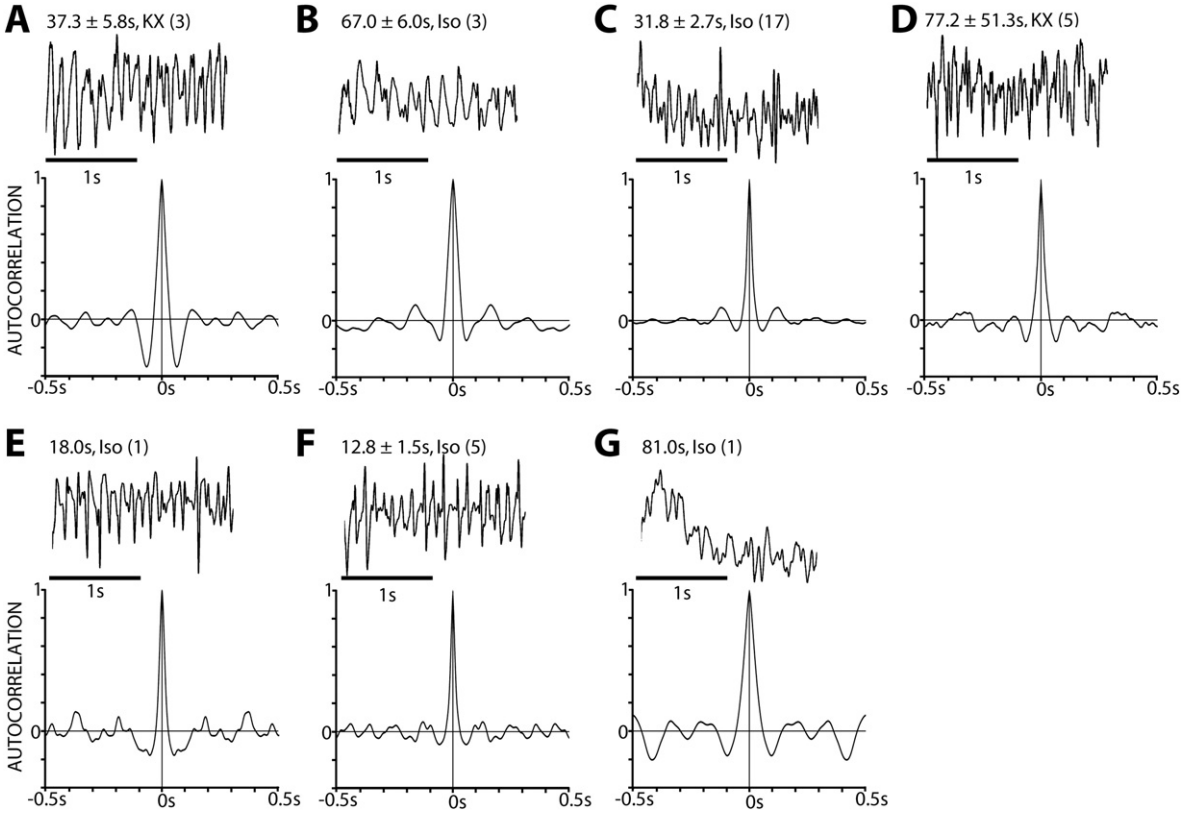


**Fig. 3.** Tonic–clonic seizures during EEG–fMRI experiments. Tonic–clonic seizures were observed in 7 animals with a mean duration of 40.1 s ± 7.7. As in Fig. 2, each panel represents data from one animal, indicating mean seizure duration ± SEM for that animal, anesthetic used (Iso, isoflurane; KX, ketamine/xylazine), and number of seizures (in parentheses). EEG traces show 2 s of representative seizure discharges from each animal. Lower traces show mean autocorrelation during tonic–clonic seizures within each animal with a lag of 0 to 500 ms, which showed substantially less periodicity than spike–wave seizures (see Methods for details).

As a measure of periodicity, the sum of the squared autocorrelation values (see Methods) were lower for tonic–clonic seizures (1.7 ± 0.36 mean ± SEM, N = 7, range 0.68–3.26) and did not overlap with the higher values seen in spike–wave seizures (15.8 ± 4.8 mean ± SEM, N = 10, range 7.2–56.1). The average tonic–clonic seizure duration was 40.1 s ± 7.7 (mean ± SEM; range 9 to 281), which was greater than short spike–wave seizures ($p \leq 0.001$, 2-sample t-test) but less than long spike–wave episodes ($p \leq 0.001$, 2-sample t-test).

*Cortical fMRI changes*

Using the same conventional SPM analysis methods employed in most human fMRI studies, we found that in all three seizure classes the cortex exhibited almost exclusively fMRI increases (Fig. 4). This differs markedly from human spike–wave seizures, where mainly cortical decreases have been observed (Aghakhani et al., 2004; Archer et al., 2003; Berman et al., 2010; Gotman et al., 2005; Moeller et al., 2008; Salek-Haddadi et al., 2003). The lack of BOLD fMRI decreases was not related to seizure duration, because both short (Fig. 4A) and long spike–wave seizures (Fig. 4B) produced similar results. For comparison, we analyzed fMRI changes in tonic–clonic seizures and also found predominantly fMRI increases with SPM analysis (Fig. 4C). After FDR correction, fMRI decreases were observed in only 0.0%, 0.3%, and 0.5% of significant voxels for short spike–wave, long spike–wave and tonic–clonic seizures, respectively. On a single animal level, fMRI decreases made up an average of 0.9 ± 0.5%, 4.3 ± 3.5%, and 5.0 ± 3.0% of FDR-corrected, significant voxels. Analysis without FDR correction at a threshold of $p < 0.05$ revealed similar proportions of fMRI decreases (data not shown).

The lack of fMRI decreases was also not related to spike–wave frequency. When spike–wave seizures were segregated based on low (2.9–4.5 Hz; Figs. 2A, B, E, F, I, J) and high (5–8 Hz; Figs. 2C, D, G, H) frequencies, both groups exhibited predominately fMRI increases (t-maps not shown), yielding decreases in 0% and 0.5% of FDR-corrected, significant voxels, respectively.

Prior work has shown that the timecourse of fMRI changes associated with spike–wave seizures may not match the standard HRF, which could lead to fMRI changes that might be missed by conventional analyses such as SPM modeling with a single HRF (Aghakhani et al., 2004; Bai et al., 2010; Carney et al., 2010; Moeller et al., 2008). To ensure that fMRI decreases in spike–wave seizures were not missed due to an unexpected timing of the changes, we repeated our initial analysis and replaced the canonical HRF with a gamma-function that peaked at 3, 5, 7, or 9 s after seizure onset. For all seizure types and peak time values, this approach showed mainly increases in cortical BOLD signal with only minimal cortical decreases (Supplemental Figs. S1–S4). We selected the HRF model with maximum decreases for each seizure type and we found that fMRI decreases were observed in only 0.06%, 0.26%, and 0.69% of significant voxels for short spike–wave (7 s gamma HRF), long spike–wave (3 s gamma HRF) and tonic–clonic (5 s gamma HRF) seizures, respectively.

As a final measure to understand BOLD changes during each seizure type, we performed a regional timecourse analysis on four cortical areas showing significant activation during ictal periods (Fig. 5A). In all four cortical regions, smaller fMRI increases were seen during short spike–wave seizures compared to long spike–wave seizures. Both types of seizures showed a gradual return towards baseline in the postictal period with no substantial fMRI decreases (Fig. 5B). Tonic–clonic seizures, which had mean durations closer to short spike–wave seizures than long (vertical dashed lines in Fig. 5B), had only slightly greater fMRI amplitude than short spike–wave seizures. However unlike short or long spike–wave seizures, postictal fMRI decreases were seen in all regions

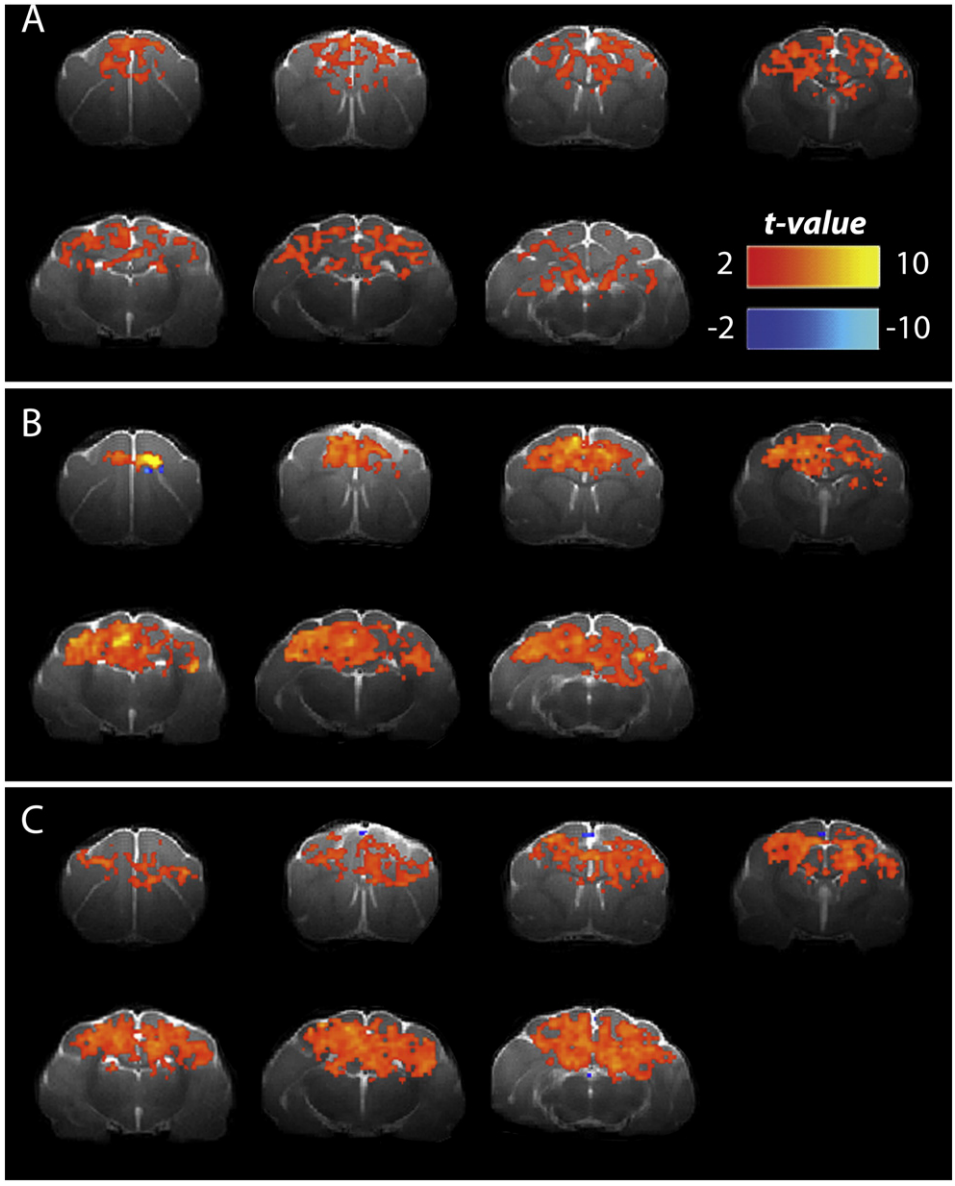


**Fig. 4.** Cortical fMRI increases and negligible fMRI decreases in ferret spike–wave and tonic–clonic seizures. Group analysis is shown across seizures with conventional HRF modeling in SPM. (A) Short spike–wave seizures (18 seizures in 4 animals). (B) Long spike–wave (17 seizures in 6 animals). (C) Tonic–clonic seizures (35 seizures in 7 animals). fMRI increases (warm colors) and decreases (cool colors) are shown with FDR-corrected height threshold $p < 0.05$. Functional data are superimposed on high resolution anatomical images from the template animal. Coronal slices are shown progressing from anterior (top left image) to posterior (bottom right image) at 2 mm intervals.

following tonic–clonic seizures, which has been noted previously in other animal models (DeSalvo et al., 2010).

A summary of peak fMRI increases and decreases in all three seizure types is shown in Fig. 6. Significant peak fMRI increases were seen during seizures in all four cortical ROIs for both spike–wave and tonic–clonic seizures (Fig. 6A). Calculation of peak postictal fMRI changes revealed no significant decreases for spike–wave seizures, but did show significant fMRI decreases for tonic–clonic seizures (Fig. 6B).

## Discussion

We found that 3–4 Hz spike–wave discharges resembling human absence seizures elicited fMRI increases in the ferret cortex without the late sustained decreases observed in human patients. These results were consistent across spike–wave seizures of different durations, different frequencies, under several anesthesia regimens, and using both conventional GLM analysis in SPM or ROI-based timecourses. In contrast, tonic–clonic seizures produced significant fMRI decreases in the postictal period as expected. These finding suggest that 3–4 Hz spike–wave discharges are not sufficient to produce fMRI decreases and other considerations are necessary to explain this phenomenon.

In principle, there are a number of possible influences that could contribute to the presence of BOLD fMRI deceases in human spike–wave seizures but not in animal models. Prior to this study, the frequency of the discharges was a logical factor to explain this finding. Earlier work investigating 3–4 Hz spike–wave seizures in the feline generalized penicillin epilepsy model has shown that each epileptiform spike is associated with increased firing of cortical neurons lasting about 100 ms or less, while the waves produce a marked decrease or complete silence of cortical neurons for nearly 300 ms (Avoli et al., 1983; Kostopoulos et al., 1981). At the timescale of fMRI measurements, which integrate the effects of neuronal activity over seconds, one can envision that the decreases in neuronal firing during the waves could dominate the average signal, leading to cortical fMRI decreases in 3–4 Hz spike–wave seizures. The 7–8 Hz spike–wave seizures in rodent models such as the WAG/Rij rat have only brief slow waves

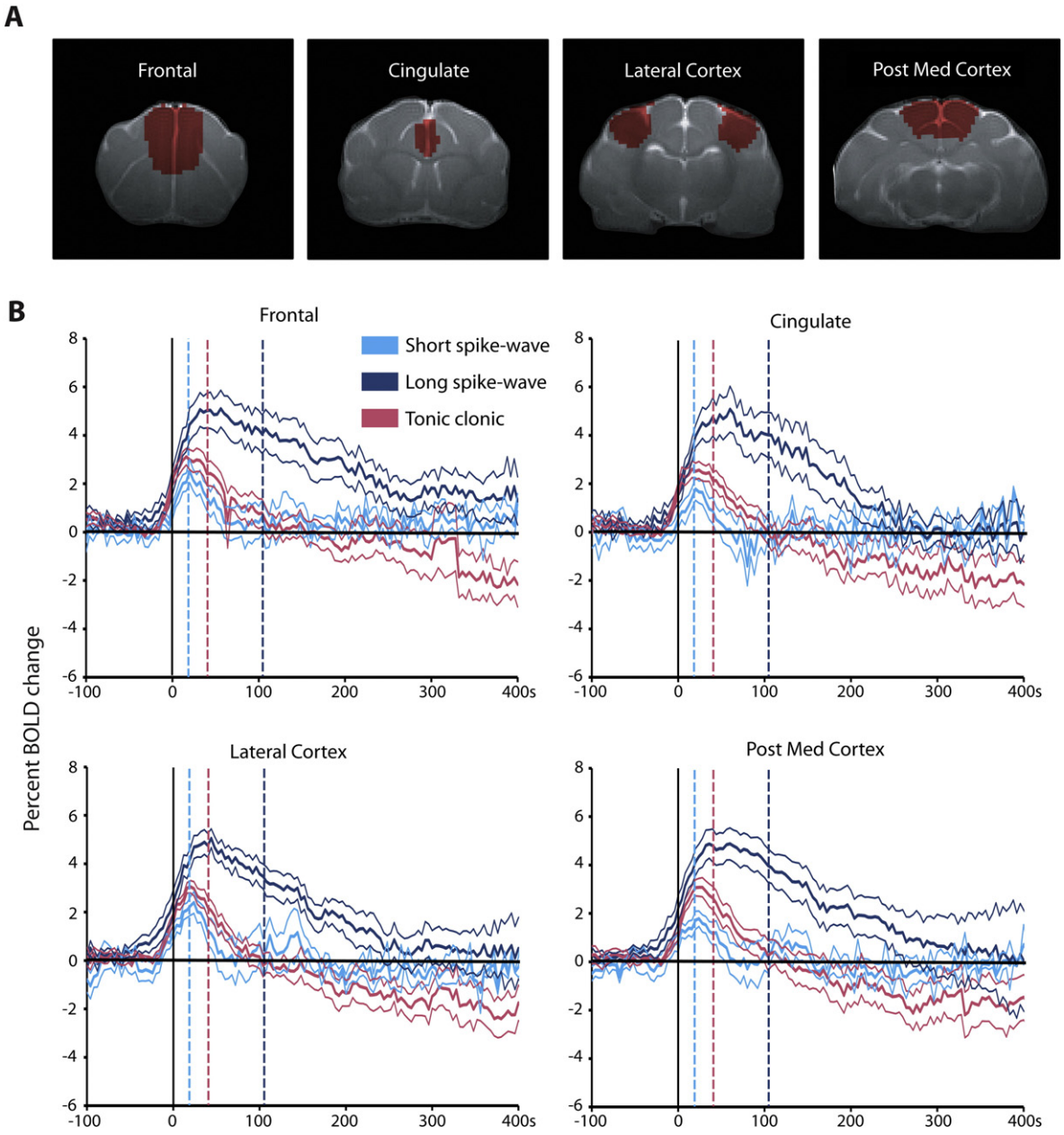


**Fig. 5.** Timecourse analysis of fMRI signals in spike–wave and tonic–clonic seizures. (A) Cortical regions of interest (ROIs) used for analysis, drawn on the template brain. (B) Spike–wave seizure fMRI timecourses show a rapid increase in activation at seizure onset followed by a gradual return towards baseline in the short (light blue trace) and long (dark blue trace) spike–wave seizures. Tonic–clonic seizures (purple trace) show fMRI increases followed by postictal fMRI decreases. Vertical dashed lines indicate the mean duration based on EEG for each seizure type. Mean signals ± SEM are shown. Data are from the same animals and seizures as in Fig. 4.

lasting 120–150 ms (Depaulis and van Luijtelaar, 2005; Sitnikova and van Luijtelaar, 2007). These discharges are associated with an increase in the firing rate of cortical neurons averaged over the time scale of seconds (Mishra et al., 2011; Nersesyan et al., 2004a, 2004b) as well as an increase in the fMRI signal (Mishra et al., 2011; Nersesyan et al., 2004a, 2004b; Tenney et al., 2004a, 2004b). While differences in discharge frequency might provide a reasonable explanation for the absence of fMRI decreases in animal models, the present study demonstrates persistence of this phenomenon in spite of seizures with a 3–4 Hz firing rate and morphology similar to humans. Therefore, differences in spike–wave discharge frequency do not explain the lack of cortical fMRI decreases in animal models.

It is also possible that the intensity of firing during the seizure's spike component could play a role. More intense firing during the spikes of ferret or rodent models could lead to fMRI increases. Less neuronal firing during the spikes in human seizures might allow the waves to dominate and cause an overall decrease in neuronal metabolism and fMRI signal. However, examples of both large and small amplitude spikes (relative to the slow waves) were observed in the ferret spike–wave discharges (see Fig. 2) with mainly fMRI increases seen in individual animals in both cases. This makes reduced spike intensity a less likely mechanism for fMRI decreases. In addition, even if neuronal activity were decreased on average during spike–wave seizures this still would not explain the prolonged fMRI decreases seen in human patients lasting over 20 s after seizure termination (Bai et al., 2010; Carney et al., 2010; Moeller et al., 2008).

Other possible explanations for the lack of cortical fMRI decreases in animal models will require further investigation. Although ferrets have sulci and gyri more closely resembling humans than the rat, other differences between these species could play a role. Seizure duration

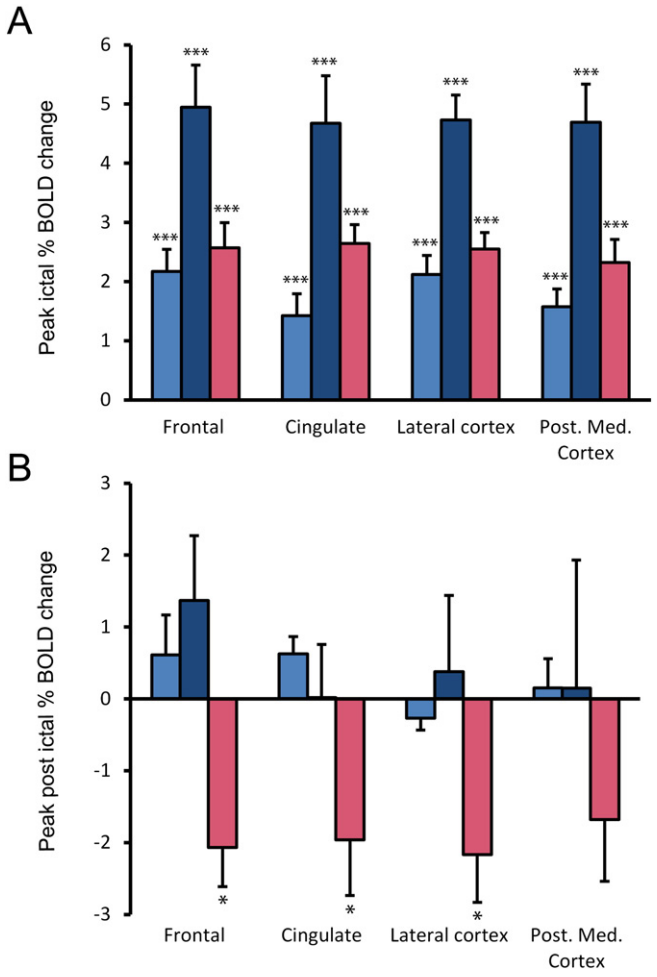


**Fig. 6.** Summary of peak fMRI changes during seizures and in the postictal period. Data and ROIs are the same as in Fig. 5. (A) Peak ictal BOLD values were calculated for each seizure type by averaging a 20 s period around the time of maximal change (see Methods for details). Values for all seizure types and ROIs were significantly different from zero (Student's t-test, $p < 0.001$, ***). An ANOVA analysis revealed a significant difference among seizure types ($F = 10.29$, $p < 0.001$). A post-hoc Tukey's test revealed that the ictal percentage change of long spike–wave was significantly greater than that of short spike–wave ($p < 0.001$), and of tonic–clonic seizures ($p < 0.001$). (B) Post-ictal BOLD changes were calculated for each seizure type by averaging percentage BOLD change in the time period of 380–400 s. BOLD decreases in tonic–clonic seizures were significantly different from zero (Student's t-test, $p < 0.05$, *) in all ROIs except the posterior medial cortex. An ANOVA analysis revealed a significant difference among seizure types ($F = 3.53$, $p < 0.01$). A post-hoc Tukey's test revealed that the post-ictal percent decrease of tonic–clonic seizures was significantly greater than that of short spike–wave ($p < 0.05$), and of long spike–wave seizures ($p < 0.001$).

alone is unlikely to be the crucial difference, since both short and long duration spike–wave seizures were seen in ferrets, as well as in human spike–wave seizures. The fact that cortical fMRI decreases were detected in the ferret model following tonic–clonic seizures makes technical or hardware-related factors unlikely as an explanation.

Another possible factor is use of analysis methods that rely on an assumed HRF, which could potentially miss fMRI decreases. A number of approaches have been used previously that place less constraints on the possible HRF (Lindquist and Wager, 2007; Lu et al., 2007). Most human fMRI studies of spike–wave seizures have used standard HRF modeling with a single canonical HRF. More recently it was shown that the complex dynamics of fMRI changes in spike–wave seizures are best revealed through more flexible approaches, including multiple gamma functions (Aghakhani et al., 2004; Bagshaw et al., 2004), sliding window (Moeller et al., 2010) and independent component analysis (Masterton et al., 2013). Most direct of all, a simple measurement of the fMRI timecourse (based on ROIs) makes no assumptions at all about the HRF (Bai et al., 2010; Carney et al., 2010). Regardless of the method used, the most consistent finding in human studies of cortical fMRI changes with spike–wave has been BOLD decreases. However, despite using three methods of fMRI analysis with the ferret model including a single canonical HRF, multiple gamma functions, and ROI-based timecourses we did not observe substantial cortical fMRI decreases. It is therefore unlikely that the analysis methods caused fMRI decreases to be missed in the ferret model.

Differences in spontaneous versus chemically-induced seizures are probably not the full explanation, because fMRI decreases were not observed in spontaneous spike–wave seizures in the genetic rat model or in chemically-induced spike–wave seizures in the ferret, but were seen following chemically-induced tonic–clonic seizures in both the rat and ferret (DeSalvo et al., 2010; Nersesyan et al., 2004a, 2004b). Nevertheless it remains possible that a combination of factors including species differences and chemical induction could lead to the observed differences from spontaneous seizures in humans.

An important final difference is that most animal fMRI studies of spike–wave have been performed under anesthesia, whereas human studies are done in the awake state. Prior work in rodent models has shown variable fMRI or cerebral blood flow changes depending on the anesthetic state (David et al., 2008; Nehlig et al., 1996; Tenney et al., 2004a, 2004b). This raises the possibility that the anesthesia used in animal models may suppress a physiological response needed to produce fMRI decreases following spike–wave seizures. We can speculate that just as the normal transition from fixation to task blocks is associated with a switch to heightened attention and cortical fMRI decreases including the default mode network (Gonzalez-Castillo et al., 2012; Gusnard and Raichle, 2001; Killory et al., 2011; Raichle et al., 2001), the transition to restored attention following seizures could induce cortical fMRI decreases by similar mechanisms. Further work will be needed to fully investigate the possible role of anesthesia and arousal state. For example, spike–wave seizures could be investigated in animal models habituated to allow fully awake fMRI to be performed, or human patients could be studied by fMRI during spike–wave seizures occurring in natural deep sleep.

In conclusion, we present a new model of generalized 3–4 Hz spike–wave seizures that closely replicates the electrographic activity of human absence seizures. This work represents the first neuroimaging study of 3–4 Hz generalized seizures on a non-primate species with well-developed sulci and gyri. To our surprise, the presence of higher cortical development and 3–4 Hz rhythmic discharge was not sufficient to produce the cortical BOLD fMRI decreases seen in human patients. Future studies will be needed to elucidate the functional mechanisms and underlying circuits involved in this phenomenon.

Supplementary data to this article can be found online at http://dx.doi.org/10.1016/j.neuroimage.2014.12.066.

## Acknowledgments

We would like to thank Bei Wang and Xiaoxian Ma for assistance during the animal surgeries. This work was supported by NIH grants R01 NS049307 and R01 NS066974 (HB), Epilepsy Foundation Postdoctoral Research and Training Award ID: 123505 (AMM), NIH grant P30 NS052519 (FH), NIH grant MSTP TG T32GM07205 (MY), and the Betsy and Jonathan Blattmachr family (HB).

## References

Aghakhani, Y., Bagshaw, A.P., Benar, C.G., Hawco, C., Andermann, F., Dubeau, F., Gotman, J., 2004. fMRI activation during spike and wave discharges in idiopathic generalized epilepsy. Brain 127 (Pt 5), 1127–1144.

Archer, J.S., Abbott, D.F., Waites, A.B., Jackson, G.D., 2003. fMRI "deactivation" of the posterior cingulate during generalized spike and wave. NeuroImage 20 (4), 1915–1922.

Avoli, M., Gloor, P., Kostopoulos, G., Gotman, J., 1983. An analysis of penicillin-induced generalized spike and wave discharges using simultaneous recordings of cortical and thalamic single neurons. J. Neurophysiol. 50 (4), 819–837.

Bagshaw, A.P., Aghakhani, Y., Bénar, C.G., Kobayashi, E., Hawco, C., Dubeau, F., Gotman, J., 2004. EEG–fMRI of focal epileptic spikes: analysis with multiple haemodynamic functions and comparison with gadolinium-enhanced MR angiograms. Hum. Brain Mapp. 22 (3), 179–192.

Bai, X., Vestal, M., Berman, R., Negishi, M., Spann, M., Vega, C., Blumenfeld, H., 2010. Dynamic time course of typical childhood absence seizures: EEG, behavior, and functional magnetic resonance imaging. J. Neurosci. 30 (17), 5884–5893. http://dx.doi.org/10.1523/jneurosci. 5101-09.2010.

Barbaresi, P., Spreafico, R., Frassoni, C., Rustioni, A., 1986. GABAergic neurons are present in the dorsal column nuclei but not in the ventroposterior complex of rats. Brain Res. 382 (2), 305–326.

Berman, R., Negishi, M., Vestal, M., Spann, M., Chung, M.H., Bai, X., . . ., Dix-Cooper, L., 2010. Simultaneous EEG, fMRI, and behavior in typical childhood absence seizures. Epilepsia 51 (10), 2011–2022.

Blumenfeld, H., McCormick, D.A., 2000. Corticothalamic inputs control the pattern of activity generated in thalamocortical networks. J. Neurosci. 20 (13), 5153–5162.

Brevard, M.E., Kulkarni, P., King, J.A., Ferris, C.F., 2006. Imaging the neural substrates involved in the genesis of pentylenetetrazol-induced seizures. Epilepsia 47 (4), 745–754.

Camfield, P., Camfield, C., 2002. Epileptic syndromes in childhood: clinical features, outcomes, and treatment. Epilepsia 43 (s3), 27–32.

Carney, P., Masterton, R., Harvey, A., Scheffer, I., Berkovic, S., Jackson, G., 2010. The core network in absence epilepsy. Differences in cortical and thalamic BOLD response. Neurology 75 (10), 904–911.

Crunelli, V., Leresche, N., 2002. Childhood absence epilepsy: genes, channels, neurons and networks. Nat. Rev. Neurosci. 3 (5), 371–382.

David, O., Guillemain, I., Saillet, S., Reyt, S., Deransart, C., Segebarth, C., Depaulis, A., 2008. Identifying neural drivers with functional MRI: an electrophysiological validation. PLoS Biol. 6 (12), 2683–2697. http://dx.doi.org/10.1371/journal.pbio.0060315.

Depaulis, A., van Luijtelaar, E., 2005. Genetic Models of Absence Epilepsy in the Rat. Elsevier Academic Press, London.

DeSalvo, M.N., Schridde, U., Mishra, A.M., Motelow, J.E., Purcaro, M.J., Danielson, N., Blumenfeld, H., 2010. Focal BOLD fMRI changes in bicuculline-induced tonic–clonic seizures in the rat. NeuroImage 50 (3), 902–909.

Ebersole, J.S., Pedley, T.A., 2003. Current Practice of Clinical Electroencephalography. Lippincott Williams & Wilkins.

Ebersole, J.S., Husain, A.M., Nordli, D.R., 2014. Current Practice of Clinical Electroencephalography. 4th ed. Lippincott Williams & Wilkins.

Englot, D.J., Mishra, A.M., Mansuripur, P.K., Herman, P., Hyder, F., Blumenfeld, H., 2008. Remote effects of focal hippocampal seizures on the rat neocortex. J. Neurosci. 28 (36), 9066–9081.

Gonzalez-Castillo, J., Saad, Z.S., Handwerker, D.A., Inati, S.J., Brenowitz, N., Bandettini, P.A., 2012. Whole-brain, time-locked activation with simple tasks revealed using massive averaging and model-free analysis. Proc. Natl. Acad. Sci. U. S. A. 109 (14), 5487–5492.

Gotman, J., Grova, C., Bagshaw, A., Kobayashi, E., Aghakhani, Y., Dubeau, F., 2005. Generalized epileptic discharges show thalamocortical activation and suspension of the default state of the brain. Proc. Natl. Acad. Sci. U. S. A. 102 (42), 15236–15240. http://dx.doi.org/10.1073/pnas.0504935102.

Gusnard, D.A., Raichle, M.E., 2001. Searching for a baseline: functional imaging and the resting human brain. Nat. Rev. Neurosci. 2 (10), 685–694.

Killory, B.D., Bai, X., Negishi, M., Vega, C., Spann, M.N., Vestal, M., Blumenfeld, H., 2011. Impaired attention and network connectivity in childhood absence epilepsy. NeuroImage 56 (4), 2209–2217 (NIHMSID #289447).

Kim, U., Sanchez-Vives, M.V., McCormick, D.A., 1997. Functional dynamics of GABAergic inhibition in the thalamus. Science 278 (5335), 130–134.

Kostopoulos, G., Gloor, P., Pellegrini, A., Gotman, J., 1981. A study of the transition from spindles to spike and wave discharge in feline generalized penicillin epilepsy: microphysiological features. Exp. Neurol. 73 (1), 55–77.

Lee, K.H., Hitti, F.L., Shalinsky, M.H., Kim, U., Leiter, J.C., Roberts, D.W., 2005. Abolition of spindle oscillations and 3-Hz absence seizure like activity in the thalamus by using high-frequency stimulation: potential mechanism of action. J. Neurosurg. 103 (3), 538–545. http://dx.doi.org/10.3171/jns.2005.103.3.0538.

Lindquist, M.A., Wager, T.D., 2007. Validity and power in hemodynamic response modeling: a comparison study and a new approach. Hum. Brain Mapp. 28 (8), 764–784.

Lu, Y., Grova, C., Kobayashi, E., Dubeau, F., Gotman, J., 2007. Using voxel-specific hemodynamic response function in EEG–fMRI data analysis: an estimation and detection model. NeuroImage 34 (1), 195–203.

Masterton, R.A., Carney, P.W., Abbott, D.F., Jackson, G.D., 2013. Absence epilepsy subnetworks revealed by event-related independent components analysis of functional magnetic resonance imaging. Epilepsia 54 (5), 801–808.

Mishra, A.M., Ellens, D.J., Schridde, U., Motelow, J.E., Purcaro, M.J., DeSalvo, M.N., Blumenfeld, H., 2011. Where fMRI and electrophysiology agree to disagree: corticothalamic and striatal activity patterns in the WAG/Rij rat. J. Neurosci. 31 (42), 15053–15064.

Mishra, A.M., Bai, X., Motelow, J.E., DeSalvo, M.N., Danielson, N., Sanganahalli, B.G., Blumenfeld, H., 2013. Increased resting functional connectivity in spike-wave epilepsy in WAG/Rij rats. Epilepsia 54 (7), 1214–1222.

Moeller, F., Siebner, H.R., Wolff, S., Muhle, H., Granert, O., Jansen, O., Siniatchkin, M., 2008. Simultaneous EEG–fMRI in drug-naive children with newly diagnosed absence epilepsy. Epilepsia 49 (9), 1510–1519. http://dx.doi.org/10.1111/j.1528-1167.2008.01626.x.

Moeller, F., LeVan, P., Muhle, H., Stephani, U., Dubeau, F., Siniatchkin, M., Gotman, J., 2010. Absence seizures: individual patterns revealed by EEG–fMRI. Epilepsia 51 (10), 2000–2010.

Motelow, J.E., Blumenfeld, H., 2009. Functional neuroimaging of spike–wave seizures. Dyn. Brain Imaging 189–209.

Nehlig, A., Vergnes, M., Waydelich, R., Hirsch, E., Charbonne, R., Marescaux, C., Seylaz, J., 1996. Absence seizures induce a decrease in cerebral blood flow: human and animal data. J. Cereb. Blood Flow Metab. 16 (1), 147–155.

Nersesyan, H., Herman, P., Erdogan, E., Hyder, F., Blumenfeld, H., 2004a. Relative changes in cerebral blood flow and neuronal activity in local microdomains during generalized seizures. J. Cereb. Blood Flow Metab. 24 (9), 1057–1068.

Nersesyan, H., Hyder, F., Rothman, D.L., Blumenfeld, H., 2004b. Dynamic fMRI and EEG recordings during spike–wave seizures and generalized tonic–clonic seizures in WAG/Rij rats. J. Cereb. Blood Flow Metab. 24 (6), 589–599. http://dx.doi.org/10.1097/01.WCB.0000117688.98763.23.

Prince, D.A., Farrell, D., 1969. 'Centrencephalic' spike–wave discharges following parenteral penicillin injection in the cat. Neurology 19, 309–310.

Raichle, M.E., MacLeod, A.M., Snyder, A.Z., Powers, W.J., Gusnard, D.A., Shulman, G.L., 2001. A default mode of brain function. Proc. Natl. Acad. Sci. U. S. A. 98 (2), 676–682.

Salek-Haddadi, A., Lemieux, L., Merschhemke, M., Friston, K.J., Duncan, J.S., Fish, D.R., 2003. Functional magnetic resonance imaging of human absence seizures. Ann. Neurol. 53 (5), 663–667.

Schridde, U., Khubchandani, M., Motelow, J.E., Sanganahalli, B.G., Hyder, F., Blumenfeld, H., 2008. Negative BOLD with large increases in neuronal activity. Cereb. Cortex 18 (8), 1814–1827.

Seneviratne, U., Cook, M., D'Souza, W., 2012. The electroencephalogram of idiopathic generalized epilepsy. Epilepsia 53 (2), 234–248.

Sitnikova, E., van Luijtelaar, G., 2007. Electroencephalographic characterization of spike-wave discharges in cortex and thalamus in WAG/Rij rats. Epilepsia 48 (12), 2296–2311.

Tenney, J.R., Duong, T.Q., King, J.A., Ludwig, R., Ferris, C.F., 2003. Corticothalamic modulation during absence seizures in rats: a functional MRI assessment. Epilepsia 44 (9), 1133–1140.

Tenney, J.R., Duong, T.Q., King, J.A., Ferris, C.F., 2004a. FMRI of brain activation in a genetic rat model of absence seizures. Epilepsia 45 (6), 576–582.

Tenney, J.R., Marshall, P.C., King, J.A., Ferris, C.F., 2004b. fMRI of generalized absence status epilepticus in conscious marmoset monkeys reveals corticothalamic activation. Epilepsia 45 (10), 1240–1247.

von Krosigk, M., Bal, T., McCormick, D.A., 1993. Cellular mechanisms of a synchronized oscillation in the thalamus. Science 261 (5119), 361–364.

Wirrell, E., Camfield, C., Camfield, P., Gordon, K., Dooley, J., 1996. Long-term prognosis of typical childhood absence epilepsy: remission or progression to juvenile myoclonic epilepsy. Neurology 47 (4), 912–918.

Wirrell, E.C., Camfield, C.S., Camfield, P.R., Dooley, J.M., Gordon, K.E., Smith, B., 1997. Long-term psychosocial outcome in typical absence epilepsy: sometimes a wolf in sheeps' clothing. Arch. Pediatr. Adolesc. Med. 151 (2), 152.